



UNIVERSITY OF LEEDS

This is a repository copy of *Measurement of Crystal Face Specific Growth Kinetics*.

White Rose Research Online URL for this paper:

<http://eprints.whiterose.ac.uk/105693/>

Version: Accepted Version

Article:

Wu, K, Ma, CY, Liu, JJ et al. (2 more authors) (2016) Measurement of Crystal Face Specific Growth Kinetics. *Crystal Growth and Design*, 16 (9). pp. 4855-4868. ISSN 1528-7483

<https://doi.org/10.1021/acs.cgd.6b00189>

© 2016 American Chemical Society. This document is the Accepted Manuscript version of a Published Work that appeared in final form in *Crystal Growth and Design*, copyright © American Chemical Society after peer review and technical editing by the publisher. To access the final edited and published work see <http://dx.doi.org/10.1021/acs.cgd.6b00189>. Uploaded in accordance with the publisher's self-archiving policy.

Reuse

Unless indicated otherwise, fulltext items are protected by copyright with all rights reserved. The copyright exception in section 29 of the Copyright, Designs and Patents Act 1988 allows the making of a single copy solely for the purpose of non-commercial research or private study within the limits of fair dealing. The publisher or other rights-holder may allow further reproduction and re-use of this version - refer to the White Rose Research Online record for this item. Where records identify the publisher as the copyright holder, users can verify any specific terms of use on the publisher's website.

Takedown

If you consider content in White Rose Research Online to be in breach of UK law, please notify us by emailing eprints@whiterose.ac.uk including the URL of the record and the reason for the withdrawal request.



eprints@whiterose.ac.uk
<https://eprints.whiterose.ac.uk/>

Measurement of Crystal Face Specific Growth Kinetics

Kui Wu^a, Cai Y. Ma^b, Jing J. Liu^a, Yang Zhang^{a*} and Xue Z. Wang^{a,b*}

^a School of Chemistry and Chemical Engineering, South China University of Technology, Guangzhou, China 510641

^b School of Chemical and Process Engineering, University of Leeds, Leeds LS2 9JT, UK

* Correspondence authors:

Personal Chair in Intelligent Measurement and Control

Institute of Particle Science and Engineering
School of Chemical and Process Engineering
University of Leeds, Leeds LS2 9JT, UK

Tel +44 113 343 2427, Fax +44 113 343 2384,
Email x.z.wang@leeds.ac.uk

Dr Yang Zhang
Lecturer

School of Chemistry and Chemical Engineering
South China University of Technology
381 Wushan Rd, Tianhe District
Guangzhou, PR China 510641
Tel: +86 20 8711 4000, Fax: +86 20 8711 4000
Email: czyzhang@scut.edu.cn

Abstract:

An instrument for measurement of face specific growth kinetics of crystals growing in a solution is developed and applied to crystallization of sodium nitrate (NaNO_3) and potassium dihydrogen phosphate (KH_2PO_4 , KDP). The device consists of three major components, a stereovision imaging system that captures in real-time the size change in each face direction of the crystal, an ATR-FTIR probe measuring solution concentration and supersaturation, and a small purpose-designed crystallizer that allows a crystal to be fixed in the solution and adequate solution mixing so the concentration measured can reflect the solution concentration near the surfaces of the crystal. The growth rates of all independent faces of NaNO_3 and KDP crystals were derived at each time interval. For the NaNO_3 crystal, growth rates in the temperature range of 298.15 ~ 318.15 K and supersaturation range of 0.01 ~ 0.11 were measured, enabling a systematic kinetic study. For the KDP crystal, the growth rates were measured just to show the capability of the system in handling crystals with different morphologies.

Keywords: non-invasive stereovision imaging, 3D shape reconstruction, face specific growth rate, sodium nitrate, potassium dihydrogen phosphate

Introduction

Crystal morphology can have a major impact on subsequent processing of crystals after crystallization such as in filtration and drying. It may also affect such properties as flowability, bulk density, drug solubility and bioavailability. Therefore engineering crystal shape and crystal shape distribution (CShD) is an important direction of research in solution crystallization^{1,2}. Advances in measurement, modeling and closed-loop control of crystal shape and CShD is recently reviewed.³

Crystal morphology can be manipulated by the type of solvents used in crystallization, crystal growth modifiers (impurities), and other operating conditions including supersaturation and stirring and mixing. An instrument that can be used to measure face specific growth rate and growth kinetics can be a useful tool in selection of solvents and in understanding the impact of crystal growth modifiers and impurities on crystal growth. They are also essential in modeling and simulation using morphological population balance models of the growth behavior for a population of crystals in a crystallization process.⁴⁻⁷

This paper describes a novel design of instrument for measuring the face specific growth rates and growth kinetics. It consists of a flowcell with a u-tube, a peristaltic pump, two thermostatic water-circulator baths with two jacket beakers and two magnetic stirrers, and a 3D imaging system and an ATR-FTIR probe. In the following, relevant previous work will be firstly reviewed, then the instrument configuration and methodology will be described in detail, followed by results and discussion section and the conclusions.

Previous work

Previous work on measurement of crystal growth kinetics will be reviewed according to the hydrodynamic conditions under which seed crystals are grown, how seed crystals are mounted, and the instrument that measures the crystal growth.

Some previous studies were carried out using growth cells where the solution remains static without mixing or flow.⁸⁻¹⁰ Such simple configuration can be achieved using a thermostatic water bath or hot-stage. Supersaturation is controlled via manipulation of solution temperature. Apparently, solute around a seed crystal would be consumed as a result of crystal growth, causing the generation of concentration gradient around the seed crystal. Agitation can be set around the seed crystal for the maintenance of a homogeneous solution condition, i.e. supersaturation in some cases. However, this

would bring a complicated flow field around the crystal, hence making it difficult to analyze the effect of solution flow on the growth of the seed crystal.¹¹ Some other work utilized pipelines to construct solution circulation system with mechanical agitation or a peristaltic pump to provide.¹²⁻¹⁵ A seed crystal was fixed onto one of the pipelines, around which the solution was generally set as laminar flow. This then made it possible to set an angle between certain crystal face and the solution flow. The influence of solution flow on the growth of seed crystals could be easily analyzed.

The seed crystal needs to be mounted, otherwise the measuring device has to move synchronously with the moving and/or rotating seed crystal, which is difficult to achieve. In literature, three methods for mounting a crystal were reported: gluing with an adhesive, fixing with external energy or force, and absorbing on a certain surface. In the first method, a solvent-proof adhesive was coated on the tip of a thin glass stick or metal wire, e.g. platinum wire, stainless steel wire, with the seed crystal sticking on it.¹⁶⁻¹⁸ The seed crystal size would not be a factor to limit the application of this method. But impurity may be introduced in the system, which may influence the underlying growth mechanism and thus growth rate of the seed crystal. In the second method, a crystal was mounted with external energy or force. Several approaches were reported. One approach is that a hot metal wire was contacted with or penetrated into the seed crystal, with the later partially melted and then crystallized and fixed on the metal wire when cooling down.¹⁵ Crystals with low melting point as well as a stable crystal form are suitable for this method as the seed crystals may not be easily changed under the high temperature of the hot metal wire. However, the seed crystals may undertake severe deformation during the melting process, which could change the crystal size and shape. In another approach the seed crystal was pierced with an extremely thin jet of water¹² or other device¹³, and then a platinum wire or string was passed through the resulting hole. Afterwards the crystal was grown for a short time period in order to fix it on the wire. Though impurity uptake can be avoided, this approach is not suitable for fragile crystals. Special clamp could also be designed to hold the seed crystal.¹⁴ However, the clamp itself could block the vision of the microscope and bring pressure for the seed crystal which can affect the crystal growth. In the third approach, crystals absorbed on the wall of the growth cell in a spontaneous nucleation process were taken as seed crystals.¹⁹ With no impurity uptake and no crystal shape destruction, this method seems to be ideal, but the position of absorbed crystals is decided by the nucleation process, which cannot be pre-set and manually changed. Success largely depends on the probability of nucleation and the capacity of the nucleus adsorption on

the vessel wall in the spontaneously nucleation process. Promising improvement of this method may be achieved by certain modification of the growth cell wall to increase the probability of nucleation on the modified site, which may be a doping of another material or change of the nanostructure of certain site on the wall surface. As we all know, surface plays an important role in heterogeneous nucleation, which enables rational design of growth cell surfaces for controlling nucleation from solution.²⁰

Measurement of single crystal growth can be classified according to the technique being offline or online. An offline method typically measures the size and weight of seed crystals at the beginning and end of the experiment, then average growth rate can be extracted.¹⁵ If the growing process is nonlinear or follows certain pattern, the off-line technique can give errors in estimation. Also, crystal sizes may change slightly in the drying process after the experiment attribute to the hygroscopicity of the crystal or mechanical damage, leading to errors in the measurement of actual crystal sizes. Online measurement provides more detailed information of crystal growing processes. An analytical balance was once used to measure weight change of a seed crystal during the growing process with the seed crystal being hanged on the balance with a string.¹¹⁻¹² Agitation was stopped temporarily when measuring the weight of the seed crystal with the solution buoyancy being reckoned. Mass growth rate of the seed crystal can be obtained in this method, but face specific growth rate cannot. Most widely used device for the online measurement of single crystal growth rate is microscope along with a CCD camera.^{8, 13-14, 18} A transparent optical window was set through which the microscope along with the CCD camera could observe and record the images of seed crystals in real time. But this method also has its limitations, that is, only a certain crystal face can be measured at a time and this face has to be parallel to the focusing plane of the camera. Other online measuring devices like Moire phase shift interferometry,¹⁷ laser interferometry,²¹ Michelson interferometer,¹⁶ and model identification approach²² were also applied in investigations of crystal growth rates and kinetics. Van Driessche et al.²³ provided an excellent review of measurement techniques of crystal growth kinetics before 2008.

The major difference of the current design of a device for measuring crystal growth kinetics is that here stereovision imaging technique is used that allows the growth rates of all individual crystal faces to be simultaneously measured. The stereovision imaging idea was proposed by Wang et al.²⁴ and tested by Ma et al.¹ and Zhang et al.²⁵ in proof-of-concept studies. The Stereovision^{NI} imaging system was developed by Pharmavision (www.pharmavision-ltd.com). The new device builds on previous work reviewed, has given detailed considerations in crystal mounting, mixing and flow.

For 1D (needles) and 2D (thin plates) single crystals, their growth kinetics can be measured by a single CCD camera providing that the crystals are parallel to the image plane of the camera. In order to demonstrate the merits of the proposed device and methodology, i.e. growth kinetics of all characteristic faces can be measured simultaneously, a 3D crystal (with at least three crystallographic independent faces) is preferred for a case study.

The selected case study chemicals for crystallization are sodium nitrate and potassium dihydrogen phosphate (KDP) with the former discussed in more detail than the later. A valuable study on the growth behavior of sodium nitrate crystals was reported by Benages-Vilau et al.²⁶, though they only examined growth rates of NaNO₃ (104) face at low supersaturations ($\sigma < 0.01$) under a narrow temperature range of 288.0 ~ 297.5 K. The influence of hydrodynamics on crystallographic equivalent (104) face was investigated. In the current study, the face specific growth rates of NaNO₃ single crystals were studied systematically under a wide supersaturation range of 0.01 ~ 0.11 and temperature range of 298.15 ~ 318.15 K. Sodium nitrate (analytical grade) was purchased from Aladdin Industrial Inc. and used without further purification. The solubility curve of NaNO₃ in water determined by Xu and Pruess²⁷ was applied in this study.

$$X = 0.0022 \times T - 0.1757 \quad (1)$$

where X represent for the mass fraction, and T is the absolute temperature. The temperature range of solubility equation (Eq. 1) is 278.15 ~ 323.15K ($R^2 = 1$).

The Device

Figure 1 is a schematic of the device. It consists of five major parts: a flowcell with a u-tube, a peristaltic pump, two thermostatic water-circulator baths with two jacket beakers and two magnetic stirrers, a 3D imaging system, and an ATR-FTIR probe.

The flowcell is made of quartz glass, with the upper side open and covered by a silicone pad. A platinum resistance thermocouple (PT100) and the crystal holder were inserted into the flowcell through the silicone pad. The seed crystal was glued on the tip of the nichrome wire (diameter 0.3 mm) on the crystal holder with a transparent epoxy adhesive. The unsaturated solution was stored in the magnetically stirred solution reservoir (Jacket Beaker 1) with its temperature being controlled by Julabo FP51-SL thermostatic water-circulator bath 1. The solution concentration was monitored and

recorded by a Mettler-Toledo ReactIR 15 ATR-FTIR probe. The solution can be circulated through jacket beaker 2, the flowcell and u-tube and back to the solution reservoir at different flow rates actuated by a BT100-2J peristaltic pump. The jacket beaker 2 served as a cooling bath which regulated the temperature (or supersaturation) of the solution to the set point when arriving at the thermocouple in the flowcell. The temperature in jacket beaker 2 was controlled by Julabo FP51-SL thermostatic water-circulator bath 2. The temperature in the flowcell can be read and recorded on a PC through the thermocouple using the Julabo EasyTemp[®] software. The 3D imaging block and LED lights were on both sides of the transparent flowcell to observe and record the growing crystal. The part of the flowcell surface not involved in the image capturing process was covered by thermal insulators to prevent temperature oscillations.

The flowcell was designed as a long narrow rectangle to ensure a steady solution flow at the seed crystal side. Thermostatic water-circulator bath 2 (the cooling bath) was used to enable the slightly undersaturated solution in the reservoir (at a relative high temperature) to become supersaturated after flowing through the cooling bath which will effectively prevent the possible burst nucleation in the solution reservoir if the solution was supersaturated. The u-tube sustains the solution level to the top of the flowcell.

The concept of 3D imaging system, which uses stereo cameras (a pair of cameras) for the reconstruction of 3D vision is directly related to the binocular vision of human beings, i.e. two cameras mimics our left and right eyes and 3D reconstruction software mimics the fast image processing of our brain. The stereo imaging system consists of a 3D imaging block (two IDS UI-2240SE-M-GL cameras with two telecentric lenses and identical specifications), a strobe control/pulse generator for synchronising cameras and lights, a light source, a light controller with strobe triggering pulse for synchronising cameras and lights, and a PC with image acquisition software and image processing software for 3D shape reconstruction and post-processing. The imaging system can capture up to 5 frames per second with each image having a resolution of 1280×1024 pixels. This pixel size represents an actual area of $3000 \mu\text{m} \times 2400 \mu\text{m}$, which is obtained through a calibration process using a $1000 \mu\text{m}$ scale plate, resulting in an actual pixel resolution of the 3D imaging system to be $2.34 \mu\text{m}/\text{pixel}$.

Application of the Device and its limitations

The seed crystal

The seed crystal mustn't exceed the vision range of the selected cameras, which is $3 \text{ mm} \times 2.4 \text{ mm}$ in size. Otherwise, cameras with wider views should be used. The size of the seed crystal in this study is about $1.0 \times 1.0 \times 0.5 \text{ mm}^3$. Seed crystal of this size is very convenient to be mounted onto the nichrome wire (diameter 0.3 mm) under 5X microscope. Smaller seed crystals are more difficult to be mounted, as it needs to be handled very carefully under a microscope with larger magnification. Since the seed crystal is glued on the crystal holder, there are no limitations on the shape of the crystal, or the number of crystal faces. But it should be noted that every characteristic face needs to have a clear view in both cameras of the system.

Orientations or angles between the crystal faces and solution flow direction could have influence on crystal growth. As a result, the seed crystals need to be fixed at a certain orientation as to ensure the comparability between experiments. The importance of crystal orientation relative to the solution flow is well documented in literature.²⁸⁻³¹ Observations of growth bands in natural galena²⁸ suggested that upstream crystal faces possess a higher growth rate, which has been confirmed in experiments on ammonium–dihydrogen phosphate (ADP)²⁹⁻³⁰. Prieto et al.³⁰ considered three orientations in the growth of ADP crystals: normal facing to the flow, parallel to the flow and in downstream position or 'in the shade'. In the 'shade' position, experiments showed lower growth rate. Sizaret et al.³¹ proposed an original model to predict crystal growth rates when volume diffusion dominates. This hydrodynamic model of diffusion through boundary layers allows to derive an analytical equation for the local growth rate along a crystal face. The main parameter controlling the final crystal shape is the angle between the face and flow direction. The growth rate decreases downstream along the faces and modifies the crystal wall orientation. In summary, fixing the orientation of the seed crystals is of great importance.

With up to 5 captured frames per second, the system can meet the needs of general crystal growth measurement. To achieve an accurate measurement requires that at least certain number of, say, 5 frames were captured during the whole growing process. With the current selection of cameras (with a view of $3 \times 2.4 \text{ mm}^2$) and seed crystals ($1.0 \times 1.0 \times 0.5 \text{ mm}^3$), the system will be accurate if the growth rate of each face does not exceed $700 \text{ }\mu\text{m/s}$. If the system is still not accurate for a certain crystal, the cameras can be replaced by high speed cameras that capture several dozen frames per sec.

The solution

The solute mass needed is decided by the solubility and concentration ranges to be examined, as well as the number of experiments to be performed. The volumes of the flowcell and solution reservoir (jacket beaker) are 30 ml and 250 ml, respectively. Accounting for the volume of the silicone pipe used, solution needed for a single experiment is about 290 ml. And solution with higher concentration can be obtained by adding the required amount of solute to the solution used in former experiment as the solute depletion caused by seed crystal growth is quite small and can be neglected. In this way, the solute depletion during the whole experiment will be reduced to the minimum. Furthermore, the volume of the solution reservoir can be adjusted by simply replacing the jacket beaker. Of course, more solution is preferred to minimize the influence of seed crystal growth on solution concentration.

If only the silicone pad and pipe and the adhesive used in mounting of the seed crystals do not dissolve in the solution, the system is applicable for any solubility system and solvent.

The adhesive

The seed crystal mustn't react with or dissolve in the adhesive used. For example, AIBN (2, 2-azobisisobutyronitrile) crystals, often used as a foamer in plastics and rubber and as a radical initiator, is soluble in the two-component epoxy adhesive used in this study. So, other mounting method or suitable adhesive should be used.

Temperature range

The silicone pad and pipe used in the system can work with a temperature range of 263.15 ~ 423.15 K. So the device should be operated within this solution temperature range. Otherwise, the parts of the device mentioned above should be replaced with better temperature resistant materials. Ambient temperature is better not to exceed the solution temperature by 5 K, because, otherwise, fog droplets will form on the surface of the flowcell due to the humidity of the environment, hence blurring the view of the CCD cameras. And a purging system (e.g. N₂) is needed to dry out the flowcell wall.

Number of experiments

The number of experiments needed to study a system is not fixed. It depends on the temperature and supersaturation ranges. In the NaNO₃ case study, 62 successful experiments at 27 conditions were carried out. As a general rule, it is better to have at least five data points to fit a curve. And within the temperature range studied (298.15 ~ 318.15 K) at least 3 temperatures should be examined (298.15 K, 308.15 K and 318.15 K). That makes 15 conditions in total. Suppose one experiment is carried out for one condition, at least 15 experiments are needed for the temperature and supersaturation ranges studied. It is suggested to have several experiments for one condition and use the average value.

Concentration Model

An attenuated total reflectance-Fourier transform infrared (ATR-FTIR) instrument, ReactIR 15 from Mettler-Toledo Ltd., was employed to monitor the NaNO₃ solution concentration in real time. The system was set to record the average value of 125 spectra every 30 s. Calibration experiments were carried out to collect data for predictive model development in advance. The calibration data used for model development contained 103 spectra with a temperature range of 278.15 ~ 363.15 K and a concentration range of 0.05015 ~ 1.35630 g/g. As shown in Table 1, every temperature value in line 1 stands for two temperatures, e.g. 10 stands for 283.15 K and 288.15 K. The data was composed of two variables sections X and Y. The X variables were the wave numbers and temperature, whereas the Y variable was the solution concentration. Figure 2 shows the ATR-FTIR spectra of sodium nitrate solution with different temperatures under a fixed concentration of 0.35g/g and different concentrations at a fixed temperature of 308.15K. The plot illustrates the dependence of IR absorbance of sodium nitrate solution on temperature and concentration, respectively. The IR absorbance of sodium nitrate solution has an apparently positive correlation with the solution concentration and an inconspicuously negative correlation with the solution temperature. The peaks at wavenumber 1356 and 1049 cm⁻¹ were chosen as the characteristic absorption bands which change significantly with the solution conditions.

Partial least square regression (PLS)^{5,32} was used to construct the predictive model of solution concentration. The data was randomly divided into two sets, the training dataset (91 spectra) for calibration model development and the test dataset (12 spectra) for model verification, which are illustrated in Table 1 as grey cells and cells with letter "v", respectively.

The R-square values of training and test data are 0.99998 and 0.99995, respectively. The prediction results of the test data are coincided with the actual values, meaning that the model works accurately. Root mean square error of prediction (RMSEP) for solution concentration of test data, using PLS models is 0.00307 g/g, which is at an acceptable level for this work.

Procedure

Preparation and Mounting of Seed Crystals

Mounting a seed crystal is another key step which distinguishes the design from previous work without solution flow.⁸⁻¹⁰ NaNO₃ seed crystals were grown by natural cooling of a saturated solution in a Petri dish at about 293 K, which takes half an hour. Crystals less than $1.0 \times 1.0 \times 0.5 \text{ mm}^3$ were picked up with tweezers onto a filter paper and the solution on the crystal surface were absorbed with a handkerchief paper, then dried and stored in a 323.15 K drying oven. The best ones were glued on the tip of a nichrome wire (diameter 0.3mm) on the crystal holder with a two-component transparent epoxy adhesive under an Olympus BX51 Microscope. This will ensure that the crystal was properly mounted on the crystal holder. Figure 3 is an illustration of the orientation of the mounted NaNO₃ crystal in the flowcell. The rhombohedral shape of the seed crystal makes it impossible to have, concurrently, a face completely parallel to the solution flow and the other one perpendicular to it. But for the convenience of 3D imaging system observation and simplicity of the NaNO₃ crystal growth hydrodynamics, the seed crystals were mounted in such a way that the (104) face parallels to the flow direction. Thus the $(\bar{1}14)$ and $(0\bar{1}4)$ faces form an angle of approximately 86° and 13° with respect to the solution flow direction, respectively, as shown in Figure 3.

Batch Experiments

For each batch experiment, the required amount of sodium nitrate and deionized water were weighted to prepare about 370g solution which was then poured into the solution reservoir (Figure 1) with a magnetic stirrer operating at a speed of 100 rpm. With the rotation rate of the peristaltic pump being 20 rpm, the solution flew through the flowcell at an average speed of 0.2016 cm/s. The resulting Reynolds number of the flow was 38.94, hence a laminar flow. The solution temperature in the reservoir was set to be 10 K higher than the setting temperature in the flowcell (measured by PT100). The temperature in the cooling bath was changed until the measured temperature in the flowcell

reached the pre-setting value. Before inserted into the flowcell, the mounted crystal was put in water for a few seconds. This will dissolve a thin layer of the crystal faces, hence avoiding the possible surface defects and contaminations as much as possible. After the insertion of the seed crystal, the position of 3D imaging block and LED lights were adjusted to obtain a good view of all three representative crystal faces. Image pairs of the growing seed crystal were captured and recorded with the 3D Stereovision^{NI} software developed by PharmaVision Ltd. at a chosen time interval (ranging from 1 ~ 100s, depending on the magnitude of the growth rate concerned). To reduce the computational time, about 50 pairs of images were chosen with equal time interval throughout each batch for performing image analysis, 3D reconstruction and post-processing to extract face specific growth rates.

Image Analysis and 3D Reconstruction

Each image of the recorded image pairs needs to experience several image processing steps including pre-processing such as the image contrast adjustment, edge/corner extraction,³³⁻³⁵ and the identification of edge/corner correspondence for 3D reconstruction. Crystals from each image of an image pair can be identified and numbered by using the multi-scale segmentation method³⁶ for further processing to obtain 3D shape information. Different features of different crystal shapes such as needle-like, plate-like, rod-like etc. were taken into account to establish corner correspondence between the identified crystal pairs, avoiding the search of the whole image to obtain the matched corners, hence improving image processing efficiency and quality.

After the stereo matching procedure, which acquired the correspondence of the identified crystal corners in the paired images, the 3D reconstruction of the crystal from the correspondence can be achieved by using the triangulation method.³⁷⁻³⁸ The 3D coordinates (X, Y, Z) of a corner is a function of the projection coordinates in the two 2D images (x_1, y_1, x_2, y_2), stereo angle (θ , 22 degrees), the total distance (L, 147.726 mm) between a subject and camera, other properties such as resolution (ω , 2.34 μm), magnification (Δ , 2 times) etc. The total distance L includes the working distance and the length of the lens, and camera flange focal distance. The obtained equation for the calculation of 3D coordinates of a corner or point from the two 2D images is as follows.¹

$$\begin{bmatrix} X \\ Y \\ Z \end{bmatrix} = \begin{bmatrix} \frac{\sin \frac{\theta}{2}}{\sin \theta} & 0 & 0 \\ 0 & 1 & 0 \\ 0 & 0 & \frac{\cos \frac{\theta}{2}}{\cos \theta} \end{bmatrix} \begin{bmatrix} \frac{L}{2} + (x_1 + x_2) \frac{\omega}{\Delta} \\ y_1 \frac{\sigma}{\Delta} \\ a + (x_2 - x_1) \frac{\omega}{\Delta} \end{bmatrix} \quad (2)$$

where $a = 54.5$ mm. With the reconstructed 3D coordinates, the crystal shape, size and their evolution, hence face specific growth rates, can be calculated.

Figure 4 is the equilibrium morphology of NaNO_3 predicted by Benegas-Vilau,³⁹ which is also obtained in this study. The six faces of a rhombohedral NaNO_3 crystal can be classified to three groups of crystallographically equivalent faces, i.e. two $\{104\}$, two $\{\bar{1}14\}$ and two $\{0\bar{1}4\}$ faces. The normal distance from the crystal center to each individual crystal face can be calculated as follows.

$$N_{(104)} = \frac{|BE|}{2\sin\beta} r \quad (3A)$$

$$N_{(\bar{1}14)} = \frac{|AE|}{2\sin\gamma} r \quad (3B)$$

$$N_{(0\bar{1}4)} = \frac{|CE|}{2\sin\alpha} r \quad (3C)$$

where

$$r = \sqrt{1 - \cos^2\alpha - \cos^2\beta - \cos^2\gamma + 2\cos\alpha\cos\beta\cos\gamma} \quad (4)$$

and the value of α , β and γ (Figure 4) are 90.57° , 102.72° and 102.72° , respectively, following Benegas-Vilau's work.³⁹ Take point B(X, Y, Z) and E(X_0 , Y_0 , Z_0) as an example, the distance between two points in 3D space can be expressed as

$$|BE| = \sqrt{(X - X_0)^2 + (Y - Y_0)^2 + (Z - Z_0)^2} \quad (5)$$

$|AE|$ and $|CE|$ can be calculated in the same way.

Results and Discussions

In order to investigate the dependence of face specific growth rates of individual NaNO₃ crystal faces on the growing environment, 62 successful batch experiments under 27 different operating conditions were conducted. The temperature range of the experiments is 298.15 ~ 318.15 K with an interval of 5 K. The corresponding relative supersaturation ranges from 0.01 to 0.11. The specific range of relative supersaturation for different solution temperatures varies depending on the metastable zone width (MSZW) at the corresponding temperature. As spontaneous nucleation happens beyond a certain supersaturation level, higher supersaturations (> 0.11) were not covered.

Calculation of Relative Supersaturation

For electrolyte solutions, the supersaturation expressed by commonly used expressions, i.e., based on the calculation from solution concentrations, may incur errors in obtaining the relationships of supersaturation and crystal growth rates. Therefore, it is necessary to incorporate the number of ions, into which a molecule dissociates, in the expressions of supersaturation.⁴⁰⁻⁴¹

The supersaturation of the solution is defined as:

$$\sigma = \frac{a_{NaNO_3} - a_{NaNO_3}^{eq}}{a_{NaNO_3}^{eq}} \quad (6)$$

where a_{NaNO_3} is the solution ionic activity of the batch experiment and $a_{NaNO_3}^{eq}$ is the activity of the solution at equilibrium or saturated status at the corresponding temperature. The numerator of Eq. 6 contains the actual value of NaNO₃ concentration in terms of molality. Solution activity is obtained through the calculation of mean activity coefficient, which is based on the work of Archer.⁴² The software PhreeqC that uses Pitzer equations⁴³ to estimate the activity coefficients could have been used, but in Archer's paper⁴⁴, it was stated that Pitzer's equations for the excess Gibbs energy per kg of water, which characterizes interactions amongst ions and solvent, occasionally give unsatisfactory representation of experimental data. So Archer provided an alternative which is a modification of Pitzer's equation, and applied it in several systems, e.g. NaBr+H₂O⁴⁴, NaCl+H₂O⁴⁵, NaNO₃+ H₂O⁴⁶. It was found by Archer that the modified Pitzer's equations fitted well with experimental data. As a result, in this study for the NaNO₃+ H₂O system, Archer's modified Pitzer models, instead of Pitzer's equations, were used.

The mean activity coefficient is calculated as a function of the solution ionic strength and its molality at the temperature of interest. The parameters used in the calculation are obtained by performing spline interpolation to the parameters between 273.15 K and 373.15 K as given in Archer's paper.⁴² Supersaturations calculated by Eq. 6 and traditional expression $\sigma = (C - C^{eq})/C^{eq}$, where C is the solution concentration and C^{eq} is the saturated solution concentration at the corresponding temperature, are both listed in Table 2 for comparison purpose.

It can be seen from Table 2 that supersaturation calculated by Eq. 6 is temperature-dependent, which is totally different from the traditional expression. It means that the same supersaturation from traditional expression differs slightly when Eq. 6 is applied at different temperatures. The slight differences may be ignored in some cases that do not need so accurate supersaturation values, hence their arithmetic mean values can be used as the batch experiments were initially designed to use the traditional supersaturation expression. However, when the supersaturation was used in the relationships with growth rates, the accurate values were applied.

3D Reconstruction and Estimation of Face Specific Growth Rates

With the left and right camera of the 3D imaging system, images of the growing seed crystal can be taken from two different directions, simultaneously. Typical image pairs obtained from a batch experiment (T: 298.15 ± 0.30 K; C: 0.94 ± 0.01 g/g; σ : 0.03067) are shown in Figure 5. The growth tendency of the seed crystal over time is quite clear. Rough surface covered the seed crystal at the initial stage due to mechanical damage or adhesive contamination in the drying and mounting processes, but it was gradually recovered to smooth surface during the process of crystal growth.

The temperature, concentration and supersaturation curves of the same experiment are shown in Figure 6. The fluctuation range of temperature in the flow cell is ± 0.3 K, which is at an acceptable level for this study. The fluctuation of solution concentration is within ± 0.01 g/g. Since ATR-FTIR probe measures the concentration of only a thin layer of solution under the ATR crystal, which is typically several microns and termed as depth of penetration,⁴⁷⁻⁴⁸ the fluctuation may be mainly caused by the solution agitated under the ATR-FTIR probe every time being slightly different from each other, though the solution concentration barely changed throughout the whole growing process. Actually, the solute consumed by the seed crystal (about 0.003 g) growth was negligible compared with the amount of circulating solution (about 370g) while no other crystals existed in the solution.

Figure 7 shows the 3D reconstructed shape evolution of a NaNO₃ seed crystal in the time range of 0 ~ 1.25 h in the same batch experiment. Figure 8 is a comparison between 3D reconstructed length and 2D projection length (left camera) of three individual NaNO₃ crystal edges. Obviously, the 3D reconstructed length is longer than 2D projection length of the same crystal edge as a whole. But for crystal edges formed by (104) and ($\bar{1}14$) faces, and (104) and (0 $\bar{1}4$) faces, i.e. (a) and (b) in Figure 8 or |EC| and |EA| in Figure 4, the 3D reconstructed lengths are just a slightly larger than the 2D projection lengths, while the former is much larger than the latter for the crystal edge formed by ($\bar{1}14$) and (0 $\bar{1}4$) faces, i.e. (c) in Figure 8 or |EB| in Figure 4. That can be easily explained by the relative angle between the camera image plane and the crystal edge. Crystal edges a and b were approximately parallel to the image plane (see Figure 5), hence the difference between the 2D projection length and the real length or 3D reconstructed length are very small. However, crystal edge c is about perpendicular to the image plane, it can be expected that the difference is quite big. The differences between the 2D projection length and the real length varies from batch to batch, because the position of 3D imaging block was adjusted slightly in order to get clear images of the seed crystal with the focal distance kept identical.

The normal distance evolution of three individual faces of a NaNO₃ crystal during the batch experiment is presented in Figure 9A with the corresponding linear fitting results as

$$N_{(104)} = 156.10444t + 111.91592 \mu\text{m} \quad R^2 = 0.98364 \quad (7A)$$

$$N_{(\bar{1}14)} = 194.91459t + 302.16265 \mu\text{m} \quad R^2 = 0.99288 \quad (7B)$$

$$N_{(0\bar{1}4)} = 239.57659t + 300.97443 \mu\text{m} \quad R^2 = 0.99131 \quad (7C)$$

where t is the time (h). Then, the face specific growth rate, i.e. the slope in the linear correlation, can be obtained. The overall crystal growth rates of three individual faces ((104), ($\bar{1}14$) and (0 $\bar{1}4$) faces) have constant values of 156.10444, 194.91459 and 239.57659 $\mu\text{m}/\text{h}$, respectively.

Effect of Mounting of Seed Crystals

The mounting of a seed crystal will inevitably insulate the mounted crystal face from the solution to some extent, hence affecting the growth of the mounted crystal face. The extent of insulation depends on the contact area of the mounted crystal face with the crystal holder, i.e. the nichrome wire

and glue. In some cases, the contact area was small and only a small part of the mounted face was occupied by the nichrome wire (Figure 10), hence the mounted face grew well. While in some other cases, the contact area was large and the nichrome wire occupied the whole mounted face, which resulted in no growth of the mounted face at all. In either case, the growth of the two $\{\bar{1}14\}$ faces, i.e. the mounted and the opposite side were not equal even though they are crystallography equivalent faces. Of course, the influence of the hydrodynamic conditions should not be ignored either. The $(\bar{1}14)$ face opposite to the mounted side faced the coming solution flow and had a higher efficiency of mass transfer, resulting in a relatively higher rate of growth unit attaching on the crystal surface, hence a higher growth rate. While the mounted face was back on to the solution flow, causing inefficient mass transfer and a relatively lower growth rate.

In order to estimate the influence of the mounted crystal holder as well as hydrodynamic conditions on the growth of the seed crystal, a growth rate ratio is defined as follows

$$\eta = \frac{L_1 - \frac{L_0}{2}}{L_2 - \frac{L_0}{2}} \quad (8)$$

where L_0 is the length of crystal edge of face (104) and $(0\bar{1}4)$ on the seed crystal, which can be seen on a grown up seed crystal in Figure 5; L_1 and L_2 indicate the distance between the seed crystal center and the mounted side and the opposite side, respectively (Figure 10). The growth rate ratio η indicates the ratio between the growth of the mounted $(\bar{1}14)$ face and the opposite crystal face. As we know, the proportions between the same two lengths are equal in a real crystal and their 2D projections. Therefore, the growth rate ratio defined in 2D images of crystals can truly represent the growth rate inequality of the real crystals.

Of all the 62 successful experiments, crystals for 34 batch experiments with clear boundaries between the rough face of the seed crystals and the rest part of the crystals were chosen to evaluate of the mounting effect on the seed crystal growth. To measure the values of L_0 , L_1 and L_2 in Eq. 10, one image of each image pairs was chosen with Image-Pro Plus software being applied. The calculated η values are shown in Figure 11 in the form of growth rate ratio vs. temperature and growth rate ratio vs. supersaturation. The growth rate ratio data are all below 1.0 but fluctuate from 0.1 to 0.9, demonstrating that the mounting of crystal holder did put a drag on the growth of the mounted crystal face. However, the extent of growth rate slowing down was not constant for different batch

experiments.

Average growth rate ratio against temperature and relative supersaturation were calculated and fitted as follows (also shown in Figure 11)

$$\eta = -0.15053 \sin(0.30896T + 42.58024) + 0.50783 \quad R^2 = 0.97751 \quad (9A)$$

$$\eta = -0.40315 \sin(50.38110\sigma + 3.54961) + 8.90123\sigma \quad R^2 = 0.96895 \quad (9B)$$

As a pure mathematical fitting, these fits do not provide any insight into the mechanism of the mounting process and hydrodynamic influence on the growth rate ratio η . As long as the R-square value is satisfactory and be sure not to be over-fitted, they are treated as good fits.

As for the two $\{0\bar{1}4\}$ faces, which are equivalent in hydrodynamic conditions and unrelated to the mounting process, their growth rate ratio is close to 1.0 in most cases. But it is difficult to confirm whether the growth rate ratio of $\{104\}$ faces is close to 1.0, because the inequality of growth in $\{104\}$ faces cannot be obtained from the current photographic direction. So it is not presented here. The influence of seed crystal size on the effect of crystal mounting was also studied, but no clear correlation between them was found. Every average growth rate ratio was the average of several values. So the tendency in the average growth rate ratio data (Figure 11) could not be a coincidence. Except for the randomness brought in by experimental operation, i.e. the contact area difference and other batch differences of experiments with the same configuration, the growth rate ratio of a batch experiment was decided by the solution temperature, relative supersaturation and the hydrodynamic conditions. Further study has to be conducted in order to get the mechanism of the mounting and hydrodynamic effect on the growth rate ratio.

Effect of Seed Crystal Size

Of the batch experiments with identical configuration, growth rates of three individual crystal faces oscillated randomly with seed crystal size. However, no clear correlation between them has been found. Considering the disperse nature of crystal growth rate, the growth rates at current experimental configuration are independent of the dimensions of the original seed crystals, within the size range studied.

Effect of Solution Velocity

Batch experiments at solution velocities ranging from 0.1031 to 0.4088 cm/s, which correspond

to the peristaltic pump rotation speed range of 10 ~ 40 rpm, at a solution temperature of 318.15 ± 0.30 K and a relative supersaturation of 0.07244, were carried out to assess the influence of solution velocities on crystal growth rates. The results are shown in Figure 12, where each data point is the average of two batch experiments.

Although the growth rates under different solution velocities fluctuated slightly with solution velocities, there is no noticeable correlation between solution velocity and the growth rate, suggesting that within the velocity range studied the growth of NaNO_3 crystals is not a diffusion-controlled process. The 20 rpm rotation speed of the peristaltic pump chosen for most batch experiments is reasonable.

Experimental Growth Rate

Figure 13 shows the face specific growth rates of NaNO_3 three individual crystal faces as a function of supersaturation and solution temperature. Each data point with error bars was the average of 2 to 4 batch experiments with the error bar indicating the standard deviation. A comparison of growth rates among three individual faces revealed that the order of growth rates was typically $(104) < (\bar{1}14) < (0\bar{1}4)$, with an average proportion of 1:1.42:1.53 (average of all batch experiments).

Typically, crystal growth rates of all faces increased along with the supersaturation at low supersaturations (head part) until a short decrease or scattering process changed the trend (scattering part), but the increasing tendency recurred thereafter (tail part). At the head part of G - σ curves, growth rates decreased with the increase of solution temperature below 308.15 K, but the dependence became scattered for the scattering part and the tail part, also for the G - σ curves at temperature above 308.15 K. Error bars of the data points of G - σ curves appeared to be shorter at both ends, i.e. head and tail parts, than the central scattering part at medium supersaturation.

Although growth kinetics of NaNO_3 can be derived from Figure 13, it seems that a single growth mechanism is inadequate due to the scattered dependence of the growth rates on supersaturation and solution temperature. In fact, a compound growth kinetic may be able to explicate all these aforementioned phenomena.

Comparison with Growth Rate Data from Literature

Growth rates of the NaNO_3 (104) face at 298.15 K, 303.15 K and 313.15 K were compared with

the growth rate data from literature and shown in Figure 14 with logarithmic coordinates. The experimental details of the literature are listed in Table 3. Our data agrees well with Treivus⁴⁹ and Oosterhof et al.⁵⁰ in both temperature and supersaturation levels, which also experienced oscillations of crystal growth rates but without agitation. Benages-Vilau et al.²⁶ also glued the seed crystal on a sample holder with roughly the same solution velocity. The growth rate data obtained is coincident with this study in magnitude, but the supersaturation range studied is below 0.01. The interesting part is that the growth rate was measured with different (104) face orientations, which were perpendicular and parallel to the solution flow, respectively, and the former is generally larger than the latter by 10-30%. The growth rate of Rossiter⁵¹ is 5~10 times of this study at the same supersaturation level and with slightly growth rate oscillations. Part of the reason is that Rossiter defined the growth rate of NaNO₃ to be the gradient of early linear part of the characteristic dimension (CD) vs. time, where the CD is the square root of the area of {104} face. Growth rate under this definition is close to (but not exactly) the geometrical average face specific growth rate of {-114} and {0-14} faces. Furthermore, the measured NaNO₃ crystal faces were not strictly parallel to the image plane of the microscope. But it is worth noting that the growth rate increases at first but gradually decelerated to a constant level after about 30 minutes in her study. The deceleration in growth was attributed to growth cell design in which the solution was stagnant, hence unable to maintain constant liquor composition, so the supersaturation decreased overtime. In fact, Rossiter's failure in keeping constant supersaturation might due to the very small amount of solution used (20g), which could be easily influenced by extra nucleation.

A fact needs to be noticed is that growth rate generally increases with the rise of temperature in literature data (Figure 14). While in our study, growth rate reduces at temperatures below 308.15K at the head part of G- σ isotherm, and then the G- σ isotherms interlaced with each other in the scattering and tail parts and the rest temperature range. Though the crossover between G- σ isotherms can be caused by mechanism competition, hence resulting in a disordered growth rates dependence on temperature, the growth decrease with the increase of temperature at the first stage may also be caused by impurities which could be induced during the crystal mounting process. Impurity caused growth rates divergence can be found in literature.⁵²⁻⁵⁵ But to confirm this hypothesis, further experiment needs to be conducted.

Monitoring the Growth of a KH_2PO_4 (KDP) Single Crystal

A second case study is monitoring the growth of a KH_2PO_4 (KDP) single crystal in an aqueous solution. Here the focus is not on the method of mounting the seed crystal by adhesive since it has been reported previously in numerous studies^{16-18, 56}. Rather it is on the capability of the proposed system on measuring crystal growth kinetics. KDP finds widespread applications in laser as a frequency doubler and has been studied in great detail.⁵⁷ Figure 15 is the diagrammatic form of the natural morphology of KDP crystal, a combination of a tetragonal prism and a tetragonal bipyramid, the angles between two crystallographic independent faces (the prismatic {100} faces and pyramidal {101} faces) are 45° .¹³ The normal distance from the crystal center to each individual crystal face can be calculated as follows.

$$N_{(100)} = \frac{|MN|}{2} \quad (10A)$$

$$N_{(101)} = \frac{\sqrt{6}}{6}|MP| + \frac{\sqrt{2}}{4}|MQ| \quad (10B)$$

Unlike for NaNO_3 , in this case study, the temperature and concentration profiles were not strictly controlled. The seed crystal was obtained from natural cooling of a saturated solution in a Petri dish at about 290 K, which took about half an hour. A seed crystal (about $1.0 \times 0.5 \mu\text{m}^2$) was absorbed with a plastic dropper and dropped into a growth cell (another Petri dish) filled with 120ml KDP aqueous solution ($\sim 0.247 \text{ g/ml}$). The solution was supersaturated at ambient temperature (about 290K) and no spontaneous nucleation occurred after the seed crystal added. The solution in the vicinity of the seed crystal was occasionally agitated manually with a glass rod to keep its uniformity. The orientation of the seed crystal was not apparently changed by the slight agitation. The 3D imaging block and LED lights were on both sides of the growth cell. Image pairs of the seed crystal were taken through the whole growing process (about 82 minutes) and 21 pairs of which with equal time interval were chosen to extract face specific growth rates using aforementioned methodology.

A sequence of image pairs of the seed crystal is shown in Figure 16. Figure 17 is the normal distance evolution of two crystallographic independent faces with the corresponding linear fitting result as

$$N_{(100)} = 13.56t + 296.71 \quad \mu\text{m} \quad R^2 = 0.9314 \quad (11A)$$

$$N_{(101)} = 118.03t + 418.54 \quad \mu\text{m} \quad R^2 = 0.9968 \quad (11B)$$

where t is time (h). The face specific growth rates of the two crystal faces ((100) and (101) faces), i.e.

the slope of the linear fitting, are 13.56 and 118.03 $\mu\text{m/h}$, respectively. This agrees with the observation of the 3D imaging system in Figure 16 that the KDP seed crystal elongated in the normal direction of pyramidal face (101), but barely grew in the normal direction of prismatic face (100).

Conclusions

An instrument for direct measurement of face specific growth kinetics of growing crystals is developed. It is based on 3D on-line imaging and real-time measurement of solution concentration using ATR - FTIR. The device is applied to crystallization of NaNO_3 , the face specific growth rates of all three independent crystal faces were obtained simultaneously. The solution circulation system driven by a peristaltic pump allows a NaNO_3 seed crystal glued on a nichrome wire and placed in a transparent flowcell to grow at homogeneous solution conditions. Growth rates obtained in this study agreed well with the literature data. Application of the instrument to monitoring the growth of a potassium dihydrogen phosphate (KDP) crystal demonstrates its capability in handling crystals with different morphologies.

The face specific growth kinetic models of crystals obtained can be integrated with a morphological population balance model⁴ to simulate the morphology evolution for a population of crystals, i.e. the so-called crystal shape distribution³. This system can also be applied to study the crystal growth behavior in different solvents and the impact of impurities and crystal growth modifiers. In the future, refractive index-based optical techniques⁵⁸⁻⁵⁹, e.g. interferometry, schlieren and shadowgraph, could be combined with the system, to obtain a concentration map in the vicinity of the seed crystal as well as the facet growth behaviour, potentially getting more insight into the influence of solution concentration on the crystal growth kinetics.

Acknowledgments

Financial supports from the China One Thousand Talent Scheme, the National Natural Science Foundation of China (NNSFC) under its Major Research Scheme of Meso-scale Mechanism and Control in Multi-phase Reaction Processes (project reference: 91434126), the Natural Science Foundation of Guangdong Province (project title: Scale-up study of protein crystallization based on modelling and experiments, project reference: 2014A030313228) as well as the Guangdong Provincial Science and Technology Projects under the Scheme of Applied Science and Technology

Research Special Funds (Project Reference: 2015B020232007) are acknowledged. The authors would like to extend their thanks to Yujiao Liu of Pharmavision (Qingdao) Intelligent Technology Limited (www.pharmavision-ltd.com) who provided the non-invasive on-line 3D imaging instrument Stereovision^{NI}.

Nomenclature

a	solution ionic activity
a, b, c	crystal edge of (104) and $(\bar{1}14)$ faces, (104) and $(0\bar{1}4)$ faces and $(\bar{1}14)$ and $(0\bar{1}4)$ faces of NaNO_3 crystals
C	solution concentration, g/g
G	face specific growth rates, $\mu\text{ m/h}$
L	total distance between a subject and camera, mm
L_0	length of crystal edge of (104) and $(0\bar{1}4)$ faces on seed crystal, μm
L_1, L_2	distance between the crystal center and the mounted face and the opposite face, μm
$N_{(101)}, N_{(100)}$	normal distance from the KDP crystal center to the (101) and (100) faces, respectively
$N_{(104)}, N_{(\bar{1}14)}, N_{(0\bar{1}4)}$	normal distance from the NaNO_3 crystal center to the (104), $(\bar{1}14)$ and $(0\bar{1}4)$ faces, respectively
R	correlation coefficient
S	solubility, g/g
T	absolute temperature, K
t	time, h
X	mass fraction
x, y	2D coordinates
X, Y, Z	3D coordinates

Greek letters

α, β, γ	angles between NaNO_3 crystal edges b&c, a&b and a&c
Δ	magnification of the camera
η	growth rate ratio between the growth of the mounted crystal face and the opposite face
θ	stereo angle of 3D imaging system, $^\circ$
σ	supersaturation
ω	resolution of the camera, μm

Subscripts and superscripts

$(104), (\bar{1}14), (0\bar{1}4)$ relates to (104), $(\bar{1}14)$ and $(0\bar{1}4)$ faces of NaNO_3 crystal

(101), (100) relates to (101) and (100) faces of KDP crystal
eq equilibrium or saturated condition

References

- (1) Ma, C. Y.; Liu, J. J.; Wang, X. Z. *AIChE J.* **2016**, 62, 18-25.
- (2) Lovette, M. A.; Browning, A. R.; Griffin, D. W.; Sizemore, J. P.; Snyder, R. C.; Doherty, M. F. *Ind.Eng.Chem.Res.* **2008**, 47, 9812-9833.
- (3) Ma, C. Y.; Liu, J. J.; Wang, X. Z. Particuology, in press. <http://dx.doi.org/10.1016/j.partic.2015.09.014> **2016**.
- (4) Ma, C. Y.; Wang, X. Z.; Roberts, K. J. *AIChE J.* **2008**, 54, 209-222.
- (5) Ma, C. Y.; Wang, X. Z. *Chem. Eng. Sci.* **2012**, 70, 22-30.
- (6) Liu, J. J.; Ma, C. Y.; Hu, Y. D.; Wang, X. Z. *Comput. Chem. Eng.* **2010**, 34, 1945-1952.
- (7) Wan, J.; Wang, X. Z.; Ma, C. Y. *AIChE J.* **2009**, 55, 2049-2061.
- (8) Nguyen, T.; Hammond, R.; Roberts, K.; Marziano, I.; Nichols, G. *CrystEngComm* **2014**, 16, 4568-4586.
- (9) Suharso, S. *Jurnal Matematika & Sains* **2009**, 10, 101-106.
- (10) Ochsenbein, D. R.; Schorsch, S.; Salvatori, F.; Vetter, T.; Morari, M.; Mazzotti, M. *Chem. Eng. Sci.* **2015**, 133, 30-43.
- (11) Bennema, P. *Phy. Status Solidi (b)* **1966**, 17, 555-562.
- (12) Rolfs, J.; Lacmann, R.; Kipp, S. J. *Cryst. Growth* **1997**, 171, 174-182.
- (13) Mullin, J.; Amatavivadhana, A. J. *Appl. Chem.* **1967**, 17, 151-156.
- (14) Lacmann, R.; Tanneberger, U. J. *Cryst. Growth* **1995**, 147, 194-199.
- (15) Botsaris, G. D.; Denk Jr, E. *Ind. Eng. Chem. Fundam.* **1970**, 9, 276-283.
- (16) Li, C.; Tsukamoto, K. J. *Cryst. Growth* **2001**, 233, 336-342.
- (17) Kanzaki, N.; Onuma, K.; Ito, A.; Teraoka, K.; Tateishi, T.; Tsutsumi, S. *J. Phys. Chem. B* **1998**, 102, 6471-6476.
- (18) Guzman, L.; Kubota, N.; Yokota, M.; Sato, A.; Ando, K. *Cryst. Growth Des.* **2001**, 1, 225-229.
- (19) Pusey, M.; Snyder, R.; Naumann, R. J. *Biol. Chem.* **1986**, 261, 6524-6529.
- (20) Diao, Y. Design of polymeric substrates for controlled molecular crystallization. Massachusetts Institute of Technology, 2012.
- (21) Yoshizaki, I.; Tsukamoto, K.; Yamazaki, T.; Murayama, K.; Oshi, K.; Fukuyama, S.; Shimaoka, T.; Suzuki, Y.; Tachibana, M. *Rev. Sci. Instrum.* **2013**, 84, 103707.
- (22) Kim, D. Y.; Yang, D. R. J. *Cryst. Growth* **2013**, 373, 54-58.
- (23) Van Driessche, A. E.; Otálora, F.; Sazaki, G.; Sleutel, M.; Tsukamoto, K.; Gavira, J. A. *Cryst. Growth Des.* **2008**, 8, 4316-4323.
- (24) Wang, X. Z.; Roberts, K. J.; Ma, C. *Chem. Eng. Sci.* **2008**, 63, 1173-1184.
- (25) Zhang, R.; Ma, C. Y.; Liu, J. J.; Wang, X. Z. *Chem. Eng. Sci.* **2015**, 137, 9-21.
- (26) Benages-Vilau, R. I.; Rubbo, M.; Calvet, T.; Cuevas-Diarte, M. A. n.; Aquilano, D. *Cryst. Growth Des.* **2013**, 13, 3419-3428.
- (27) Xu, T.; Pruess, K. Thermophysical properties of sodium nitrate and sodium chloride solutions and their effects on fluid flow in unsaturated media; Lawrence Berkeley National Laboratory, Berkeley, CA: 2001; pp 1-48.
- (28) Kesler, S. E.; Stoiber, R. E.; Billings, G. K. *Econ. Geol.* **1972**, 67, 19-24.
- (29) Prieto, M.; Amoros, J. *Bull. Mineral.* **1981**, 104, 114-119.
- (30) Prieto, M.; Paniagua, A.; Marcos, C. *Eur. J. Mineral.* **1996**, 8, 987-996.
- (31) Sizaret, S.; Fedioun, I.; Barbanson, L.; Chen, Y. *Geophys. J. Int.* **2006**, 167, 1027-1034.
- (32) Wold, S.; Sjöström, M.; Eriksson, L. *Chemom. Intell. Lab.* **2001**, 58, 109-130.
- (33) Canny, J. Pattern Analysis and Machine Intelligence, *IEEE Transactions on* **1986**, 679-698.
- (34) Gonzalez, R. C.; Wintz, P. Digital image processing. Prentice Hall International: 2001.
- (35) Harris, C.; Stephens, M. In A Combined Corner and Edge Detection, Proceedings of The Fourth Alvey Vision Conference, 1988; pp 147-151.
- (36) De Anda, J. C.; Wang, X.; Roberts, K. *Chemical Engineering Science* **2005**, 60, 1053-1065.

- (37) Hartley, R.; Zisserman, A. Multiple view geometry in computer vision. Cambridge university press: 2003.
- (38) Trucco, E.; Verri, A. Introductory techniques for 3-D computer vision. Prentice Hall Englewood Cliffs: 1998; Vol. 201.
- (39) Benages-Vilau, R. I. Growth, Morphology and Solid State Miscibility of Alkali Nitrates. Universitat de Barcelona, 2013.
- (40) Mullin, J.; Söhnel, O. Chem. Eng. Sci. **1977**, 32, 683-686.
- (41) Kim, S.; Myerson, A. S. Ind. Eng. Chem. Res. **1996**, 35, 1078-1084.
- (42) Archera, D. G. J. Phys. Chem. Ref. Data **2000**, 29, 1141-1156.
- (43) Pitzer, K. S. J. Phys. Chem. **1973**, 77, 268-277.
- (44) Archer, D. G. J. Phys. Chem. Ref. Data **1991**, 20, 509-555.
- (45) Archer, D. G. J. Phys. Chem. Ref. Data **1992**, 21, 793-829.
- (46) Archer, D. G. J. Phys. Chem. Ref. Data **2000**, 29, 1141-1156.
- (47) Mudunkotuwa, I. A.; Al Minshid, A.; Grassian, V. H. Analyst **2014**, 139, 870-881.
- (48) Vigano, C.; Ruyschaert, J.-M.; Goormaghtigh, E. Talanta **2005**, 65, 1132-1142.
- (49) Treivus, E. Cryst. Res. Technol. **1997**, 32, 963-972.
- (50) Oosterhof, H.; Geertman, R.; Witkamp, G.; van Rosmalen, G. J. Cryst. Growth **1999**, 198, 754-759.
- (51) Rossiter, A. J. Solubility and crystal growth of sodium nitrate from mixed alcohol – water solvents. Curtin University, 2009.
- (52) Kubota, N.; Yokota, M.; Mullin, J. W. J. Cryst. Growth **1997**, 182, 86-94.
- (53) Booth, A. H.; Buckley, H. E. Nature **1952**, 169, 367-368.
- (54) Sangwal, K. Prog. Cryst. Growth Charact. Mater. **1996**, 32, 3-43.
- (55) Davis, K. J.; Dove, P. M.; De Yoreo, J. J. Science **2000**, 290, 1134-1137.
- (56) Kubota, N.; Otsuka, H.; Doki, N.; Yokota, M.; Sato, A. J. Cryst. Growth **2000**, 220, 135-139.
- (57) Rashkovich, L. N. KDP-family single crystals. CRC Press: 1991.
- (58) Srivastava, A.; Muralidhar, K.; Panigrahi, P. K. Prog. Cryst. Growth Charact. Mater. **2012**, 58, 209-278.
- (59) Verma, S.; Shlichta, P. J. Prog. Cryst. Growth Charact. Mater. **2008**, 54, 1-120.

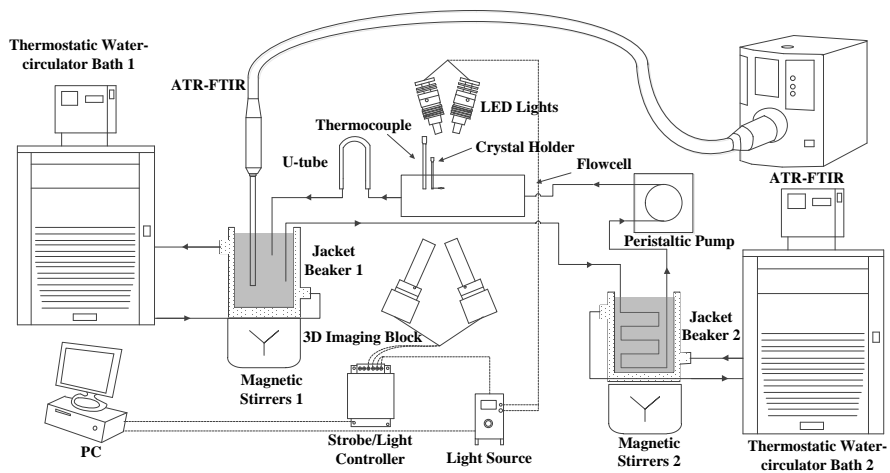


Figure 1. A schematic of the face specific crystal growth kinetics measuring device

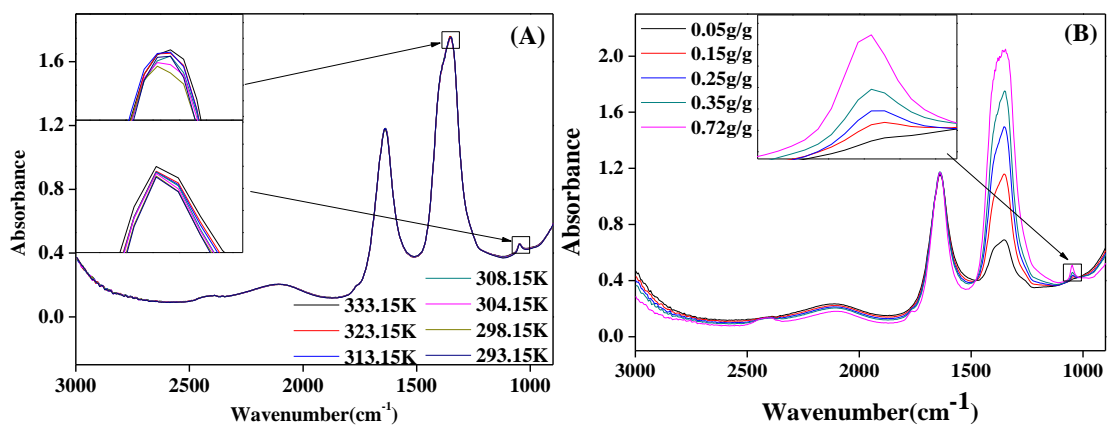


Figure 2. ATR-FTIR spectra of sodium nitrate solution with (A) different temperatures under a fixed concentration of 0.35 g/g and (B) different concentrations at a fixed temperature of 308.15 K.

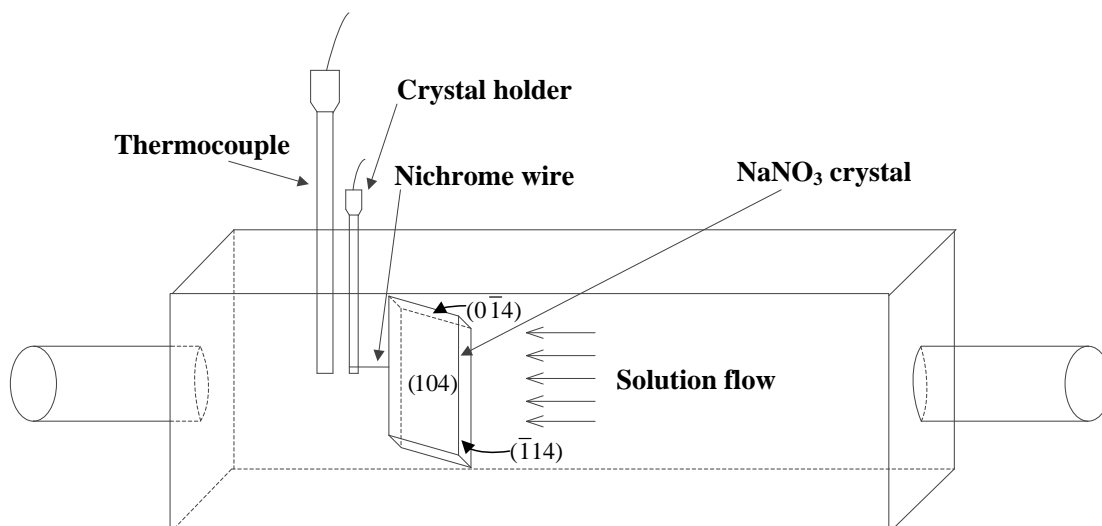


Figure 3. A diagram of a magnified NaNO_3 crystal mounted on the crystal holder to show the orientation of the crystal in the growth cell

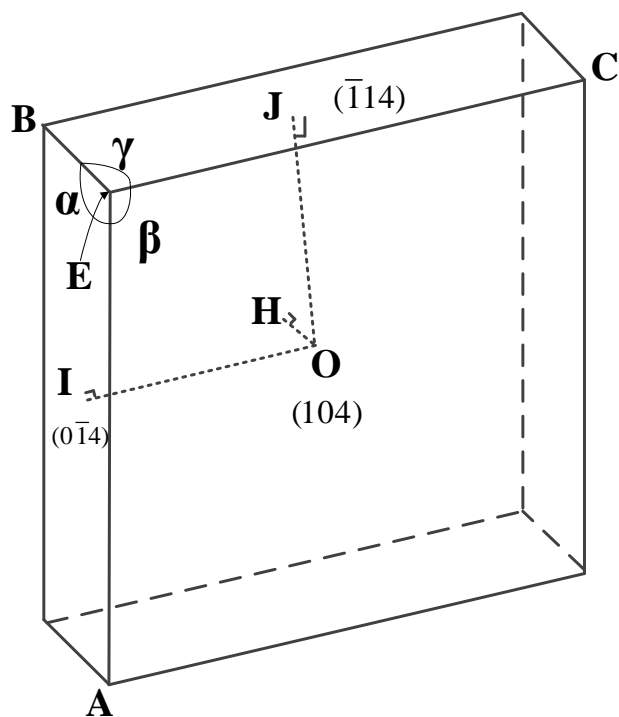


Figure 4. Equilibrium and experimental morphology of a NaNO_3 crystal

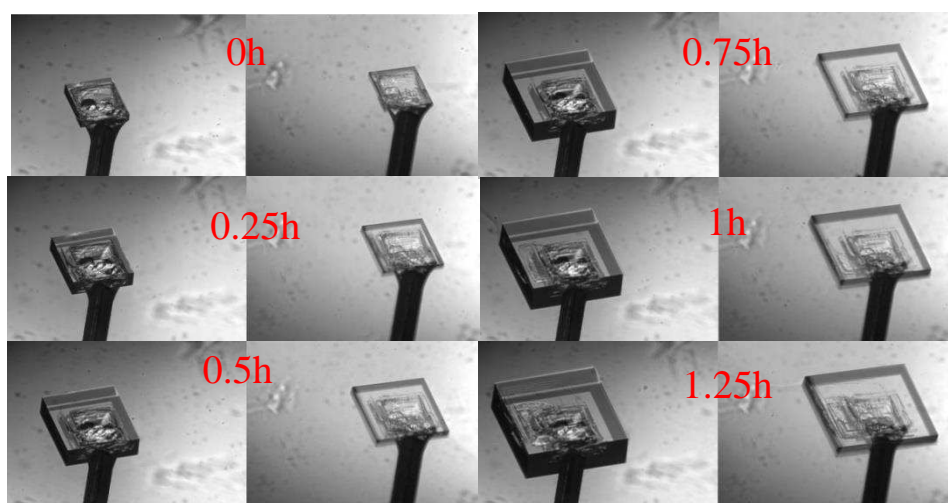


Figure 5. A sequence of image pairs (left camera and right camera) obtained from a batch experiment ($T: 298.15 \pm 0.30 \text{ K}$; $C: 0.94 \pm 0.01 \text{ g/g}$; $\sigma: 0.03067$) with the 3D imaging system.

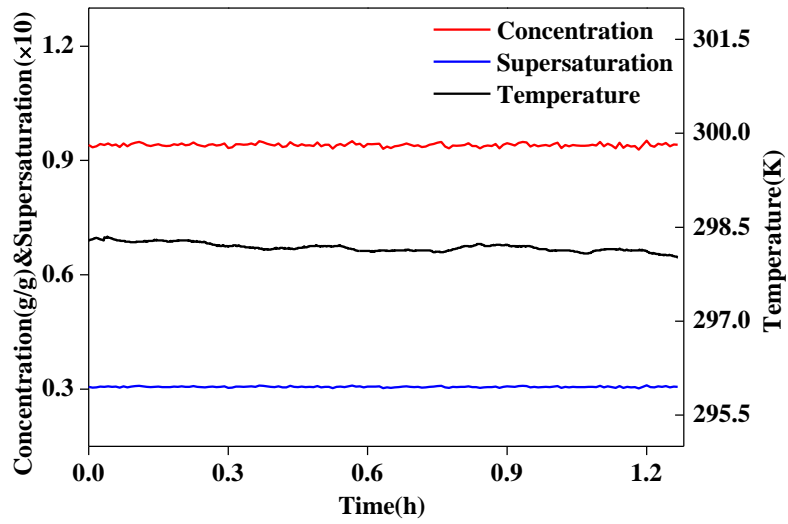


Figure 6. Temperature, concentration and supersaturation curves of a batch experiment (T: 298.15 ± 0.30 K; C: 0.94 ± 0.01 g/g; σ : 0.03067)

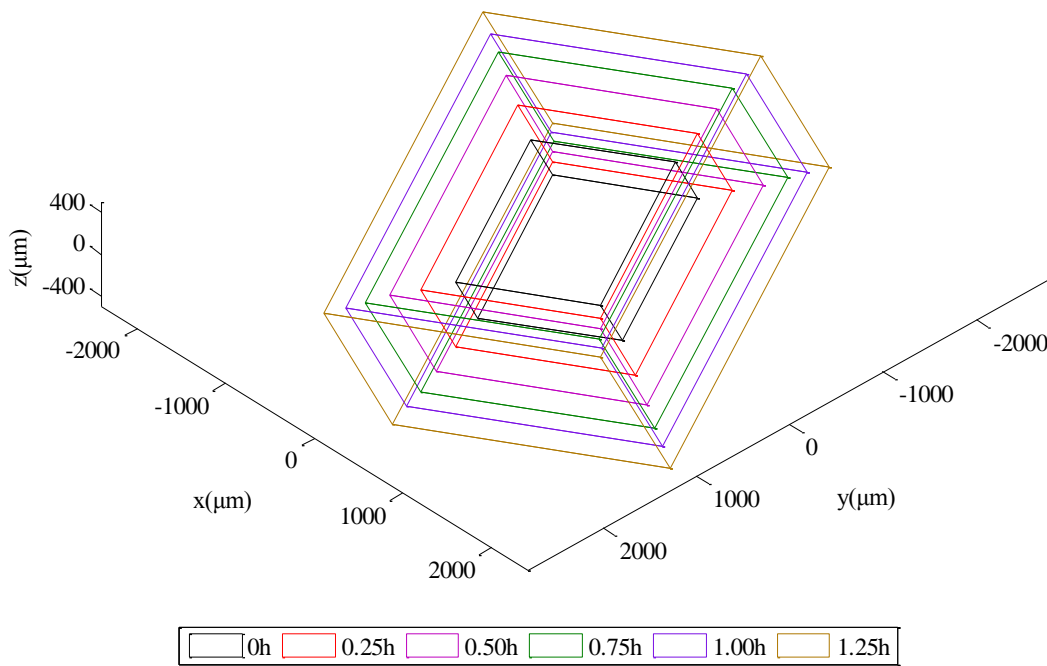


Figure 7. 3D reconstructed crystal shape evolution of the NaNO₃ seed crystal from 0 h to 1.25 h in a batch experiment (T: 298.15 ± 0.30 K; C: 0.94 ± 0.01 g/g; σ : 0.03067)

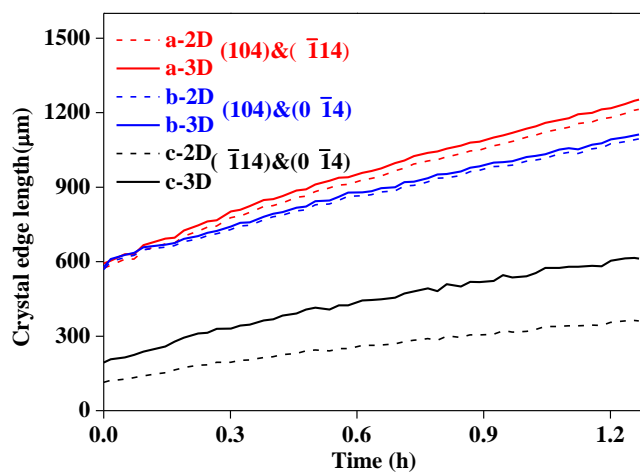


Figure 8. Comparison between 3D reconstructed lengths and 2D projection lengths (left camera) of individual NaNO_3 crystal edges (lines - 3D reconstruction lengths, dots - 2D projection lengths)

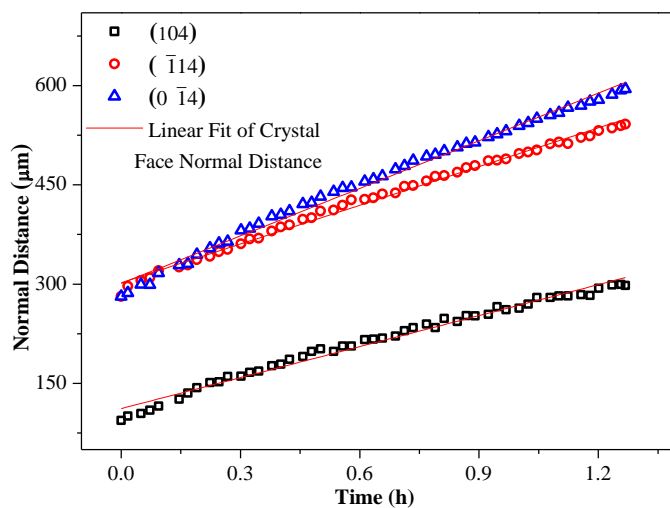


Figure 9. Normal distance evolution of three individual faces of a NaNO_3 crystal with a linear fit

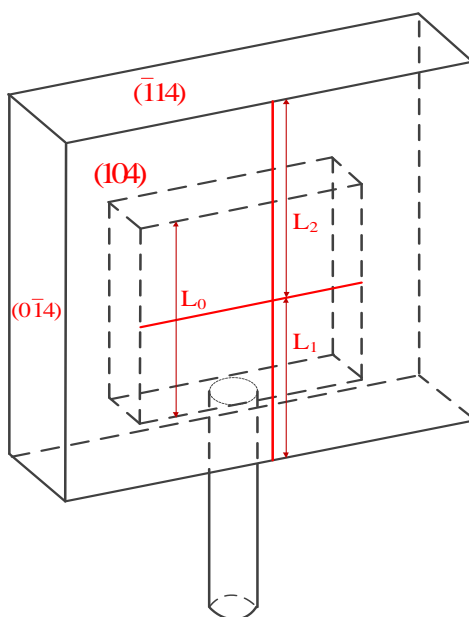


Figure 10. Outline of 2D image of the mounted NaNO_3 crystal grew on the basis of the seed crystal.

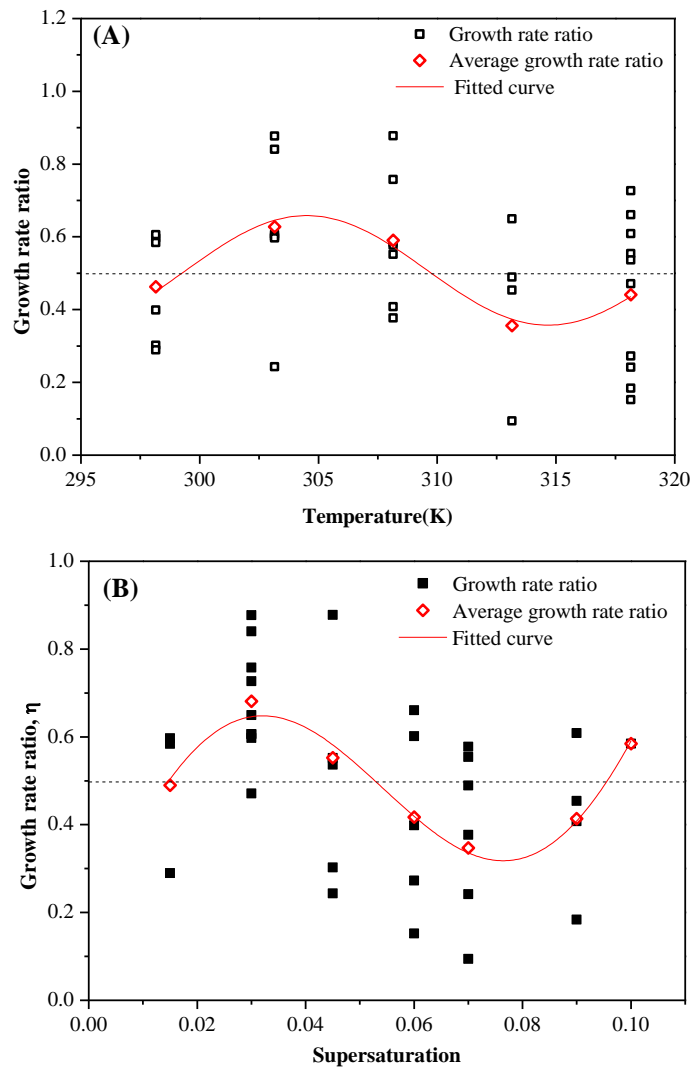


Figure 11. Calculated growth rate ratio values of 34 batch experiments shown in the form of (A) Growth rate ratio vs. Temperature and (B) Growth rate ratio vs. Supersaturation. (Dashed lines indicate the growth rate ratio of 0.5.)

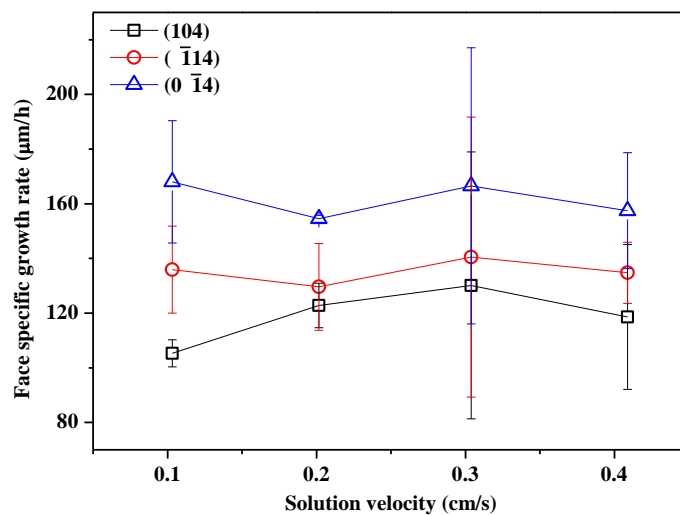
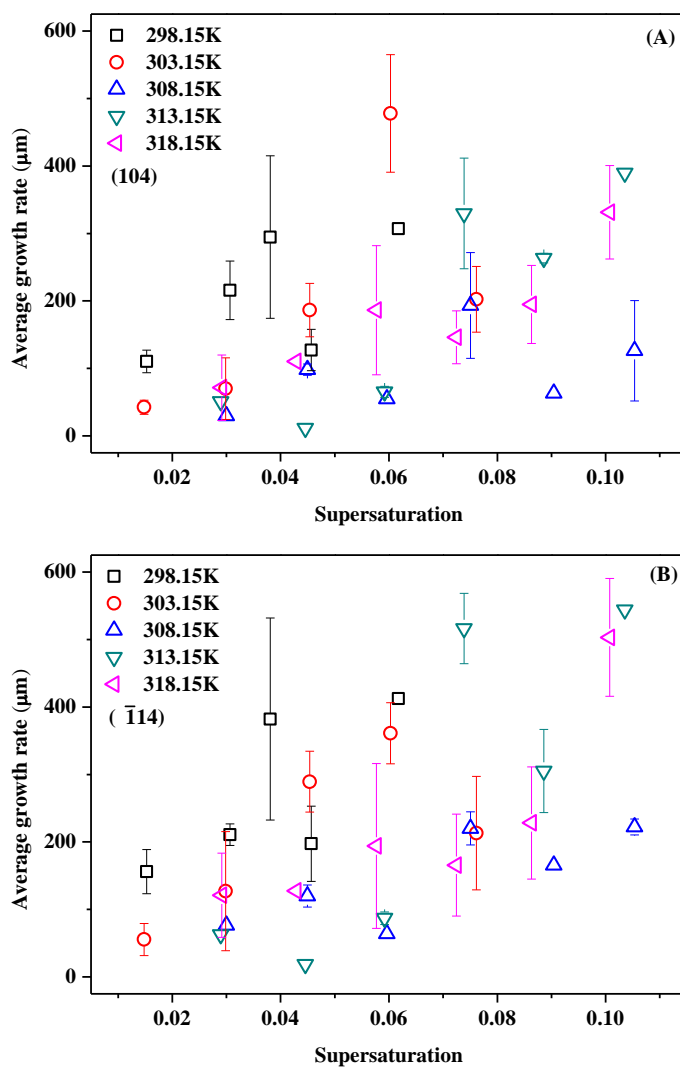


Figure 12. Face specific growth rates of NaNO₃ crystals under different solution velocities. (T: 318.15 ± 0.30 K; C: 1.16 ± 0.01 g/g; σ: 0.07244.)



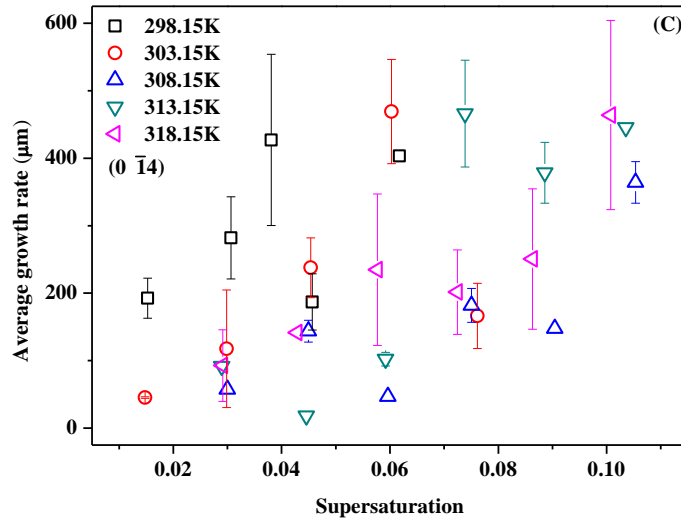


Figure 13. Face specific growth rates of three individual crystal faces of NaNO_3 crystals vs. supersaturation and temperature

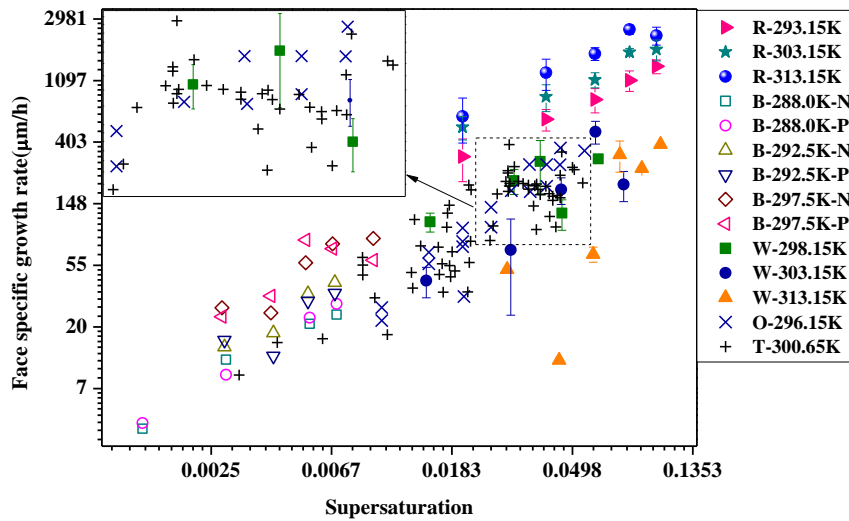


Figure 14. Comparison of NaNO_3 (104) face growth rates in this study with data from Treivus⁴⁹, Oosterhof et al⁵⁰, Rossiter⁵¹ and Benages-Vilau et al.²⁶, which is prefixed by the letter “W”, “T”, “O”, “R” and “B” in the legend, respectively. The suffixes “N” and “P” in the legend represent growth rate measured with the (104) face perpendicular and parallel to the solution flow, respectively. The axes are in their natural logarithmic form.

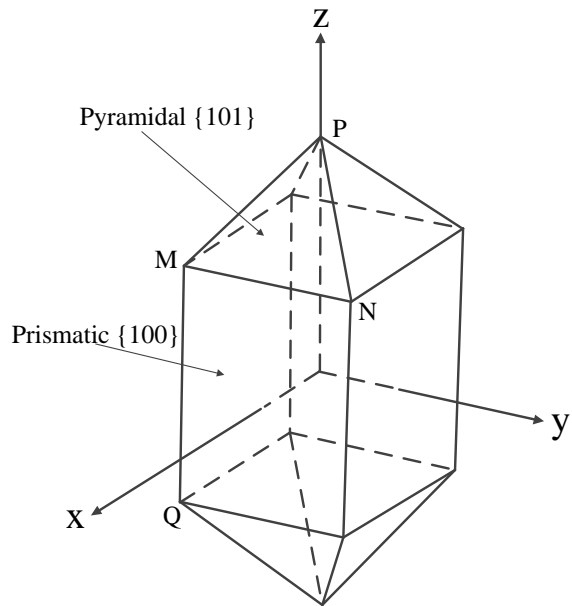


Figure 15. Morphology of a KDP crystal

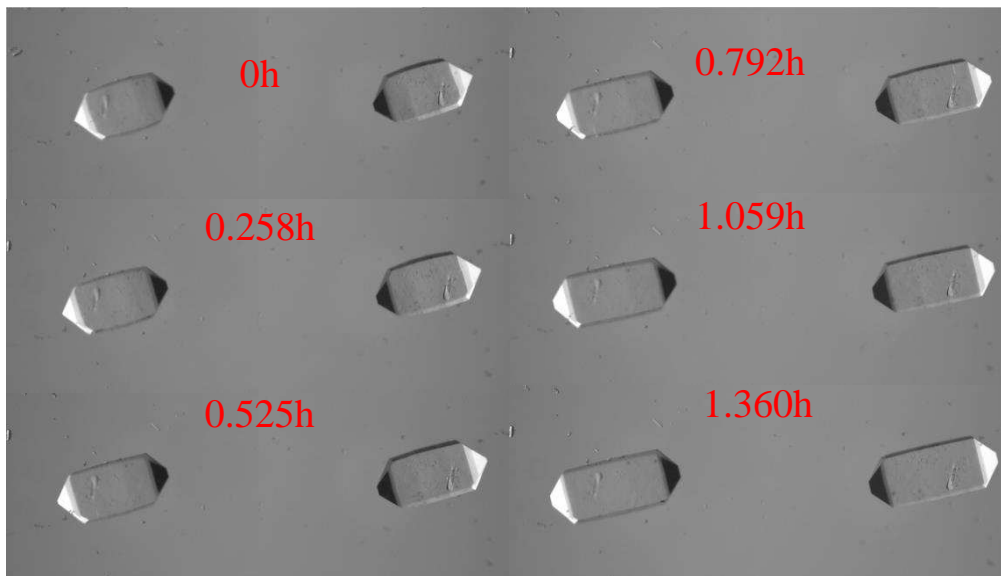


Figure 16. A sequence of KDP crystal image pairs (left and right camera) obtained from a batch experiment (T: ~290 K; C: ~ 24.7 g/ml)

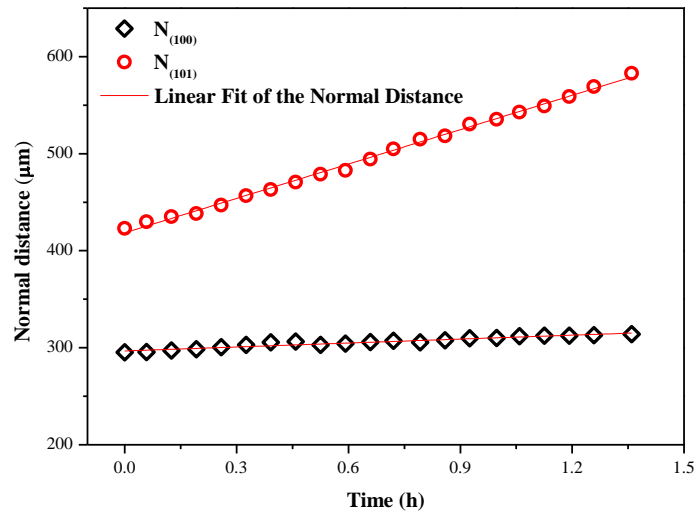


Figure 17. Normal distance evolution of two crystallographic independent faces of the KDP crystal with a linear fit

Table 1. Calibration data collection at different sodium nitrate concentrations and solution temperatures

Temperature(-273.15K)	5	10	20	30	40	50	60	70	80	90
Concentration(g/g)										
0.05015					v					
0.15155						v				
0.24948				v						
0.35147					v					
0.49837					v					
0.71992							v			
0.79853								v		
0.87128									v	
0.92110								v		
1.12520							v			
1.24740									v	
1.35630										v

Table 2. Supersaturations of experimental NaNO₃-H₂O solution calculated by different expressions

Temperature(K)	Supersaturation						
$\sigma=(C-C^{eq})/C^{eq}$	0.01	0.02	0.03	0.04	0.05	0.06	0.07
298.15	0.01528	0.03067	0.04568	0.06173			
303.15	0.01478	0.02984	0.04536	0.06028	0.07616		
Eq.6 308.15	0.01496	0.02998	0.04497	0.05962	0.07503	0.09043	0.10533
313.15		0.02896	0.04455	0.05918	0.07387	0.0886	0.10354
318.15		0.02914	0.04288	0.05770	0.07244	0.08634	0.10074

Table 3. Experiment details in the literature

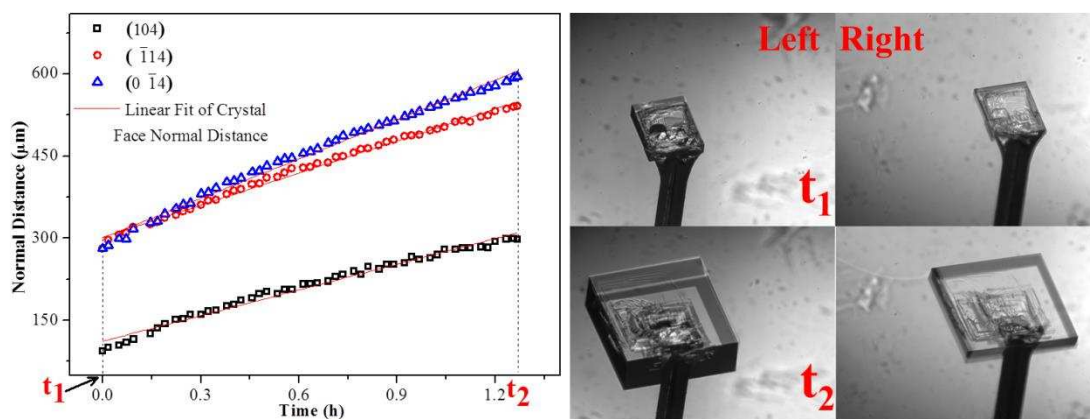
Reference	Amount of solution	Growth cell size	Seed crystal size	Seed mounting	Number of crystals*	Solution velocity	Measuring device
⁵¹	20g	5ml	~0.2-0.5mm	NA	6-26	0-8.82ml/min	Microscope
²⁶	1600g	0.6×1 cm ²	<2×2×1 mm ³	Glued	10	40ml/min	Microscope
⁴⁹	~60ml	60ml	0.1-1.5 mm ³	NA	1	No agitation	Microscope
⁵⁰	NA	NA	<0.5 mm	Unfixed	1	No agitation	Microscope
Here	~370g	3×1×10 cm ³	<1×1×0.5 mm ³	Glued	1-4	36.29 ml/min	3D imaging

*Number of crystals means number of crystal measured to get one growth rate data.

For Table of Contents Use Only

Measurement of Crystal Face Specific Growth Kinetics

Kui Wu, Cai Y. Ma, Jing J. Liu, Yang Zhang and Xue Z. Wang*



Synopsis

An instrument based on 3D imaging for measurement of face specific growth rates of growing crystals and ATR-FTIR for concentration measurement is developed. Image pairs of growing NaNO_3 and KH_2PO_4 seed crystals were captured in real time in two different directions. After image analysis and 3D reconstruction operation, crystal growth kinetics of individual faces can be derived.